High-Performance Visualization for Ocean Modeling

Wael H. Ali[a], Youran Gao[b], Corbin Foucart[a], Manan Doshi[a], Chris Mirabito[a], Patrick J. Haley, Jr.[a], Pierre F. J. Lermusiaux[a, †]

[a] *Department of Mechanical Engineering, Massachusetts Institute of Technology, Cambridge, MA*

[b] *Department of Earth, Atmospheric and Planetary Sciences, Massachusetts Institute of Technology, Cambridge, MA*

[†]Corresponding Author: pierrel@mit.edu

OCEANS 2022, Hampton Roads | 978-1-6654-6809-1/22/$31.00 ©2022 IEEE | DOI: 10.1109/OCEANS47191.2022.9977075

***Abstract*—Real-time sea experiments often involve large computational costs and software development associated with running numerical ocean simulations. Effective visualization tools that interpret the results of these simulations are therefore a necessity, and must overcome the challenges of plotting large, high-resolution, three-dimensional, time-dependent, and probabilistic ocean fields and associated quantities in real-time. Although disparate visualization tools aimed at ocean forecasting exist, a complete, integrated visualization suite that is efficient, interactive, and has 3D capabilities is still needed. In this work, we present the MSEAS high-performance visualization suite for real-time sea experiments. It processes multidisciplinary oceanographic fields in a computationally efficient manner and creates easy-to-use, portable, and interactive visualizations. The suite includes static visualization tools based on NCAR Graphics and MATLAB; the interactive web-based tool 2DSeaVizKit built using leaflet and D3.js for interactive 2D visualization on the world map; and 3DSeaVizKit, a browser-based, interactive 3D visualization tool built using Plotly and WebGL for exploratory 3D analysis of ocean forecasts. It can provide standard 2D cross-sections for scalar-valued data; quiver plots, pathlines, and streamtubes for vector-valued data; Lagrangian products (such as trajectories, Lagrangian Coherent Structures, etc.); isosurfaces for 3D data; and an interactive graphical user interface for selecting the quantities, times, and sub-domains of interest. We showcase applications of the visualization suite during three recent exercises that took place in the Gulf of Mexico, the Clarion-Clipperton Fracture Zone in the Pacific Ocean, and the Balearic sea.**

***Index Terms*—Ocean modeling, ocean visualization, interactive visualization, spatiotemporal data, three-dimensional, probabilistic forecasting, real-time, data assimilation**

I. Introduction

Effective visualization of oceanographic fields is crucial to understanding ocean phenomena. Such visualizations are also crucial for scientists and engineers that predict and design for the complex and harsh ocean environment [1–3]. Moreover, visualizations of oceanographic data are of practical concern to those working in shipping [4], disaster management [5], off-shore oil operations [6], and aquaculture [7]. However, visualization of oceanographic fields is not without its challenges. Measured data sets are sparse and heterogeneous, while modeling data sets are often large (available for multiple depths, multiple time instants, multiple domains, and multiple realizations) [8, 9]. Both types of data, i.e., measured and modeled data, are multivariate (e.g., temperature, salinity, velocity) and may contain uncertainties, noise, and discontinuous data [10–12]. These complexities necessitate oceanographic visualization tools with the capacity to handle multi-dimensional, multi-resolution, and multi-dynamics models to produce interpretable visualization maps. Such tools must also balance the resolution-speed tradeoff when used in real-time ocean modeling to deliver visualizations quickly and efficiently, possibly remotely, without incurring any errors due to down-sampling from the model to the plotting resolution [8, 13].

The most common approach to oceanographic data visualization involves plotting multiple 2D lateral or depth-wise cross sections, whereby the users select the region and times they wish to plot at the software level, and use the static output plots to interpret forecast or hindcast results [14, 15]. Such 2D maps provide flexibility and ease of use which make them a compelling option for real-time forecasting experiments. However, ocean dynamics studies can benefit from a 3D visualization tool which allows the user to view the entire flow across different depths, rather than having to visualize a 3D data field from 2D cross sections [8, 16]. Several 3D flow visualization tools such as VisIt [17] and ParaView [18] have been developed for 3D flow visualization. However, these general purpose tools often lack support for complex stratified and multidisciplinary ocean data visualization, which makes them challenging for use during real-time experiments [8].

An additional feature that is crucial for effective ocean visualization is interactivity, as it allows the user to explore the ocean fields in several areas of interest and at different times. However, existing 2D and 3D interactive tools such as Met.3D [19], MEVA [20], and W3DX [21] have been restricted to meteorology, and only a few tools such as Ocean Data View [22] and VAPOR [23] have been developed for interactive ocean visualization.

In this work, we present the MSEAS visualization suite, a collection of 2D and 3D multivariate tools that produce static and interactive maps of ocean fields and quantities provided by the Multidisciplinary Simulation, Estimation, and Assimilation Systems (MSEAS). The various tools are based on the NCAR Command Language (NCL) [24] and MATLAB [25], in addition to the in-house 2DSeaVizKit [13] and 3DSeaVizKit [26] tools that we developed to offer an interactive user experience. The tools showcased in this work have been used for multiple

real-time sea exercises. This paper highlights the features of our visualization suite and its use in exploring the ocean fields and guiding our scientific results for three sea experiments that took place in the Pacific Ocean, the Gulf of Mexico, and the Balearic Sea.

The rest of this paper is organized as follows. In section II, we outline the MSEAS-PE ocean modeling system used for our simulations and the visualization methodologies employed. In section III, we provide use cases in real-time sea exercises and multiscale ocean modeling. Finally, we provide conclusions attained from the development, deployment, and use of our visualization suite in section IV.

II. Methodology

A. MSEAS-PE Ocean Model

In this work, we utilize the MSEAS primitive equation (PE) modeling system for our ocean simulations [2, 3]. The MSEAS-PE software system is used for fundamental research and for realistic simulations in varied regions of the World Ocean [27–33]. Among the model's strengths is its ability to simulate (sub)-mesoscale processes over regional domains with complex geometries and varied interactions, using an implicit two-way nesting/tiling scheme [2]. The specific subsystems used in this work include initialization schemes [3], nested data-assimilative tidal prediction and inversion [34], fast-marching coastal objective analysis [35], subgrid-scale models [36, 37], and advanced data assimilation [38, 39]. While the MSEAS-PE has been used and validated in numerous applications and sea exercises, we focus on three recent exercises in this work: (i) understanding and estimating the Gulf of Mexico Loop Current system in 2011 (GOM Hindcast 2011); (ii) forecasting plume dynamics, Lagrangian transports, and coherent sets in the Clarion–Clipperton Fracture Zone in real-time in 2021, with applications to deep-sea mining (DSM Forecast Experiment 2021); and (iii) forecasting subduction in the Balearic Sea in real-time in 2022 (DRI-CALYPSO Forecast Experiment 2022). These use cases are discussed in section III.

B. Static Visualization Suite

Due to the ease of use and portability of static plots in real-time sea experiments, the MSEAS visualization suite produces 2D static figures of ocean fields using the NCAR Graphics library [40] and MATLAB [25] developed functionalities. The generated figures include the standard two-dimensional depth, latitude, and longitude cross-sectional renderings of the scalar-valued data of ocean physics (temperature, salinity, velocity magnitude, etc.) and prognostic quantities (sound speed, vorticity magnitude, etc.), in addition to quiver plots for vector-valued data such as the barotropic or surface velocities. Our visualization suite is also equipped with in-house-developed functionality to visualize statistical and uncertainty fields such as mean, standard deviation, and higher moments of a quantity [41], as well as Lagrangian products maps of drifter trajectories, flow maps, finite-time Lyapunov exponents [42, 43], dilation maps [44], and subduction dynamics [45].

C. Interactive Visualization Suite

1) 2DSeaVizKit: For our 2D interactive visualizations, we developed 2DSeaVizKit [13], a browser-based tool used for visualizing the MSEAS-PE ocean products. The toolkit makes use of the Leaflet [46] and D3.js [47] JavaScript libraries and visualizes the multivariate, multidimensional fields obtained from the MSEAS software on the world map. The software interface is built with interactivity as a central goal, with a web interface for the user to select the selected fields, times, and depths, while ensuring a seamless transition between the forecast products, making it portable for real-time applications and decision making, both on land and at sea. The scalar-valued data are presented on 2D depth cross-sections overlaid on an interactive map. For the visualization of vector-valued data, 2DSeaVizKit uses animated pathlines which allow for visually-intuitive interpretations of the velocity field across the time window of interest.

2) 3DSeaVizKit: In this work, we utilize 3DSeaVizKit [26] to produce 3D interactive visualizations that facilitate the discovery and interpretation of 3D features in ocean dynamics. The 3DSeaVizKit software consists of two main parts, a Python pre-processing pipeline and a web-based interactive visualization suite built on top of Plotly [48]. The pre-preprocessing pipeline performs data extraction, interpolation, and masking of the raw MSEAS-PE model outputs in netCDF format and transforms the data into a format more conducive to be served over a network. The web-based front-end visualization interface presents the ocean model data using a number of methods, including isosurfaces and flat cross-sections for scalar-valued data, streamtubes and cones for vector-valued data, and path lines for trajectory data. To allow for increased flexibility and ease of use, the graphical user interface provides the user on-the-fly customization features with the option to alter the visualization appearance, such as colormap and colorbar limits. Furthermore, the rendering limits of the domain can also be changed interactively, and a time-stepping slider can be used to animate the visualization once the plots are rendered at the desired configuration.

III. Use Cases

This section showcases uses of the MSEAS visualization tools during hindcasts and real-time forecast experiments from three multidisciplinary ocean modeling projects led by our MSEAS group and collaborators. The modeling domains for these sea experiments are shown in figure 1. Table I lists the locations and resolutions of the main modeling domains employed in each experiments.

A. GOM Probabilistic Hindcast 2011

Our visualization suite was used during a probabilistic hindcast experiment for the Gulf of Mexico as part of a multi-institutional collaborative project to achieve better understanding of the Loop Current and Loop Current eddy separation dynamics. The geographic modeling domain is shown in figure 1a. One of the probabilistic modeling domain had a horizontal resolution of $1/12.5^\circ$ (about 9 km), using a

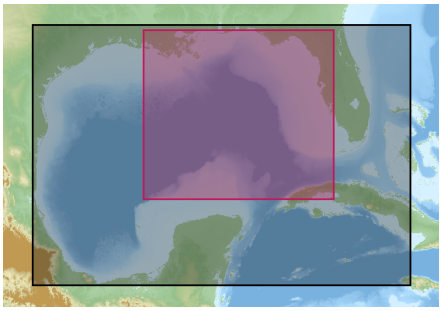

(a) GOM domain

(b) DSM domain

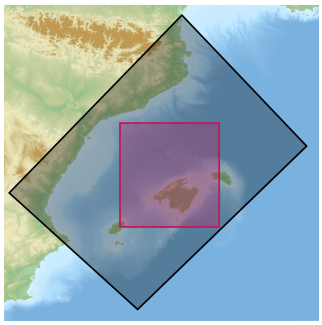

(c) DRI-CALYPSO domain

Fig. 1: Modeling domains for (a) the GOM hindcast, which includes the Gulf of Mexico and surrounding areas of the Atlantic ocean, (b) the DSM forecast experiment, located in the Clarion-Clipperton Fracture Zone in the Pacific Ocean, and (c) the DRI-CALYPSO forecast experiment, located in the Balearic sea. The red regions indicate sub-domains of interest. The topography and bathymetry data were obtained from the GEBCO_2022 grid [49].

TABLE I: MSEAS modeling domain locations, horizontal resolutions, and grid sizes for each of the sea experiments.

Sea Experiment	Location	Horizontal Resolution	Grid size
GOM	Gulf of Mexico	≈ 9 km	158×230, 100 vertical levels
DSM	Clarion-Clipperton Fracture Zone	600 m, with 200 m nest	174×179, 100 vertical levels
DRI-CALYPSO	Balearic Sea	900 m, with 300 m nest	424×573, 70 vertical levels

158×230 grid with 100 vertical terrain-following levels. The time window of interest spanned the period from June 26 to September 24, 2011.

For this experiment, we carried out a probabilistic analysis of the Loop Current dynamics, and so a 500-member ensemble hindcast was created for the three-month period of interest. The probabilistic ocean forecasts were initialized from HYCOM [50], downscaled to higher resolution. Ensemble forecasts were initialized using ESSE procedures [51, 52], extended to multi-region uncertainty initialization. Each ensemble member was forced by stochastically perturbed atmospheric flux fields from either the Climate Forecast System (CFS) 0.2° model from NCEP [53] or the ECMWF Reanalysis v5 (ERA5) 0.2° model from ECMWF [54], as well as by tidal forcing from TPXO8 [55, 56], but adapted to the high-resolution bathymetry and coastlines [34].

For this experiment, the MSEAS visualization suite was used for uncertainty fields. In particular, the mean and standard deviation fields were plotted using NCAR Graphics 2D depth and vertical cross-sections. The cross-section along 87.5°W of the standard deviation of the temperature field is shown in figure 2 at 12Z on July 26, 2011 (35 days into the hindcast) and at 12Z on September 24, 2011 (95 days into the hindcast). This figure highlights the growth of the uncertainty from the shelf and slope to the deeper levels. 2DSeaVizKit was used to further investigate this process by plotting depth sections of the standard deviation of the temperature field at 100 m and 2000 m depth as shown in figure 3 for the final time snapshot at 12Z September 24, 2011. The animated pathlines feature in 2DSeaVizKit proved to be useful in this case as it suggests that the large uncertainties are highly correlated to the flow field, particularly near the Loop Current (which can be seen in figure 3a as entering the Gulf through the Yucatán Channel and exiting through the Florida Strait) and the eddies.

3DSeaVizKit was then used to construct a three-dimensional picture of this dynamics. Figure 4 shows hindcasts of the uncertainties in the velocity field at the two time instants for the region of interest highlighted in red in figure 1a. These uncertainties are shown in terms of horizontal cross-sections of the standard deviation at 1 m and 191 m, and a vertical cross-section located along 90°W. In addition, streamtubes, a 3D extension of streamlines, of the mean velocity field at the surface are shown. Altogether, figure 4 provides better understanding of the uncertainty growth process whereby uncertainties at the surface are shown to be driven by the surface eddies, and mixing effects highlighted by the vertical section are shown to carry these uncertainties to deeper levels.

B. DSM Plume Forecast Experiment 2021

Our visualization suite was used during a real-time at-sea experiment in the Clarion–Clipperton Fracture Zone (figure 1b) in the eastern north Pacific Ocean, which took place from April 16 to May 9, 2021 [57]. The seafloor in this area is a place of active research in deep-sea mining (DSM) due to polymetallic mineral concentrations that form on the sea bottom. The process of mining the deposits and taking the ore to the surface results in the formation of metal-laden plumes, which are advected away from the mining site by the ocean velocity field. The region is also characterized by abundant biodiversity, containing organisms and ecosystems that can be affected by seabed mining [58, 59]. To estimate the impacts of these operations in the midwater realm and abyssal habitats, sediment plume models can quantify the spatial and temporal scales of mining operations. While most environmental research focuses on the seafloor, where the most direct effects will occur, plumes and other impacts of

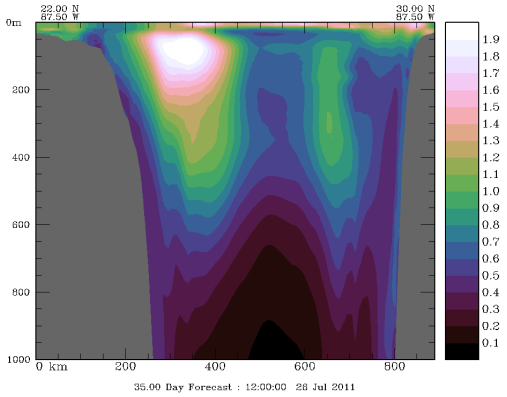

(a) Hindcast for: 12Z July 26, 2011

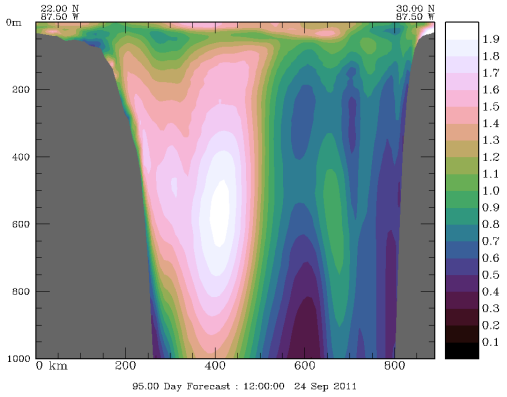

(b) Hindcast for: 12Z September 24, 2011

Fig. 2: GOM Probabilistic Hindcast 2011. Uncertainty visualization examples obtained using NCAR Graphics for the 500-member ensemble hindcast experiment. (a) and (b): hindcasts of the standard deviation of the temperature field in a longitude cross-section along 87.5°W at 12Z July 26, 2011 and 12Z September 24, 2011, respectively, as computed using the ESSE MSEAS-PE probabilistic modeling system.

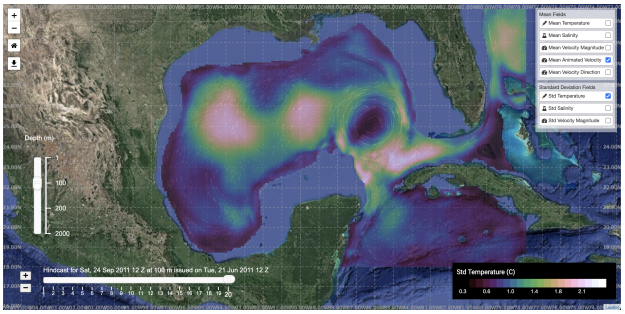

(a) Standard deviation of temperature at 100 m depth

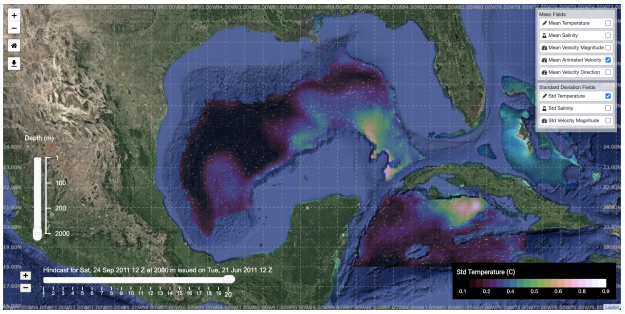

(b) Standard deviation of temperature at 2000 m depth

Fig. 3: GOM Probabilistic Hindcast 2011. Uncertainty visualization examples obtained using 2DSeaVizKit for the 500-member ensemble hindcast experiment, as computed by our ESSE MSEAS-PE probabilistic modeling system. (a) and (b): hindcasts of the standard deviation of the temperature field at 100 and 2000 m, respectively. Additionally, animated pathlines describing the mean velocity field are shown at both depths. All fields are plotted at 12Z on September 24, 2011.

seafloor mining are likely to be extensive in the water column, motivating the sea exercise.

The MSEAS modeling system was set up in an implicit 2-way nesting configuration (600 m resolution influence domain and a 200 m resolution process domain). The plume concentration is simulated as a point source with a representative volumetric flow rate. As with previous experiments, the ocean forecasts were initialized from HYCOM [50], downscaled to higher resolution and corrected based on sparse local data. Ensemble forecasts were again initialized using ESSE procedures [51, 52], extended to multi-region uncertainty initialization. These ocean simulations were forced by atmospheric flux fields forecast by the Global Forecast System (GFS) 0.25° model from NCEP [60] and by tidal forcing from TPXO8 [55, 56], but adapted to the high-resolution bathymetry [34].

1) Plume Visualization: The plume concentration is visualized in a top-down manner using the NCAR graphics library at 16Z on May 8th, 2021, 3 days into the forecast, depicted in figure 5. From the visualization, it is clear that the contents of the plume are advected by the background flow field to form a long, thin filament that stretches far from the initial source of the plume.

This approach is well-complemented by the 3DSeaVizKit rendering of the plume at 16Z on May 8th, 2021 (figure 6), which shows the variation of the plume concentration depth-wise in the water column, as well as the interaction of the sediment plume with the bathymetry and nearby seamount. The interactive, 3D nature of the 3DSeaVizKit visualization is able to convey a more visually comprehensive view of the sediment transport that would not be possible by rendering cross-sectional visualizations alone, due to the eventual meandering with 3D advection and mixing of the sediment plume. Furthermore, the ability to add or remove a representation of the full 3D velocity field to the visualization allows for the portrayal of a more dynamic interaction between the velocity field and the plume transport as compared to the top-down rendering.

2) Uncertainty Visualization: In addition to our deterministic ocean and plume forecast itself, the sensitivity of ocean flow dynamics to small perturbations presents a clear

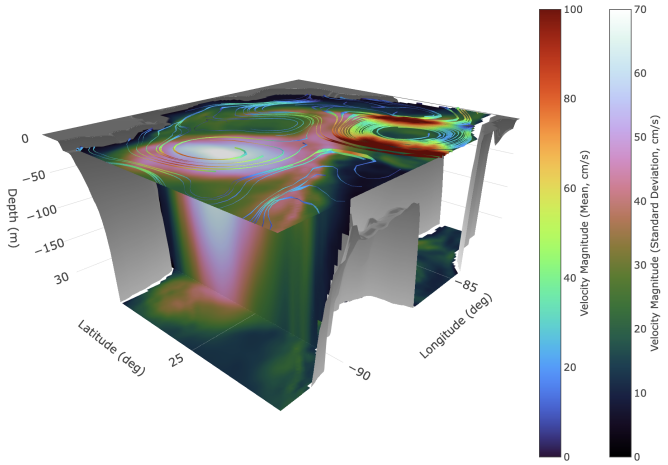

(a) Hindcast for: 12Z July 26, 2011

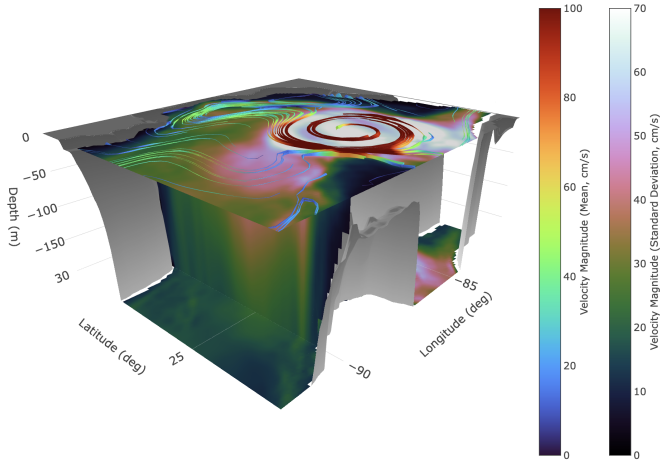

(b) Hindcast for: 12Z September 24, 2011

Fig. 4: GOM Probabilistic Hindcast 2011. Uncertainty visualization examples obtained using 3DSeaVizKit for the ensemble hindcast experiment, as computed by our ESSE MSEAS-PE probabilistic modeling system. (a) and (b): hindcasts of the uncertainties in the velocity field at 12Z July 26, 2011 and 12Z September 24, 2011, respectively. The horizontal cross-sections shown correspond to the standard deviation of the velocity field and are located at 1 m and 191 m depth, and the vertical cross-section is located along 90°W. Additionally, streamtubes of the mean velocity field are shown at the surface.

need to quantify and visualize uncertainty—a need which is magnified in light of the goal of the experiment: to assess possible regional effects of seabed mining. The uncertainty in plume concentration, as quantified by our ensemble standard deviation fields, is shown in figure 7; note that the uncertainty is plotted on a larger domain than the 3D domain used to visualize for the individual deterministic realization. From the figure, we can see that the ensemble forecast indicates a region of high uncertainty around the point source, which expands in time. This indicates that, although the individual deterministic realization presented as a long thin filament, the region potentially impacted by the plume is much larger, and

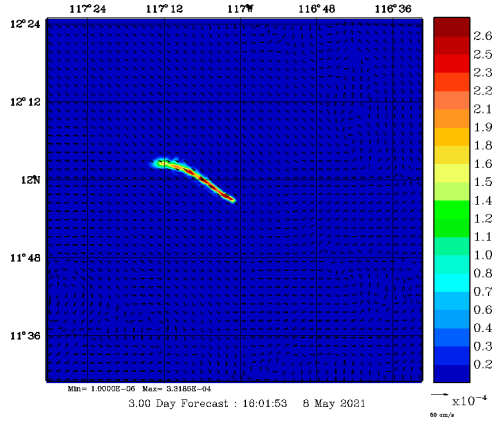

Fig. 5: DSM Plume Forecast Experiment 2021. NCAR visualizations of the sediment plume concentration, as forecast by the MSEAS-PE modeling system at 16Z on May 8th, 2021.

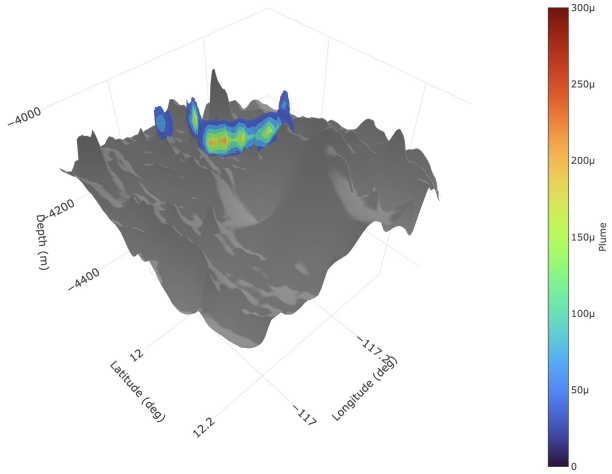

(a) View 1

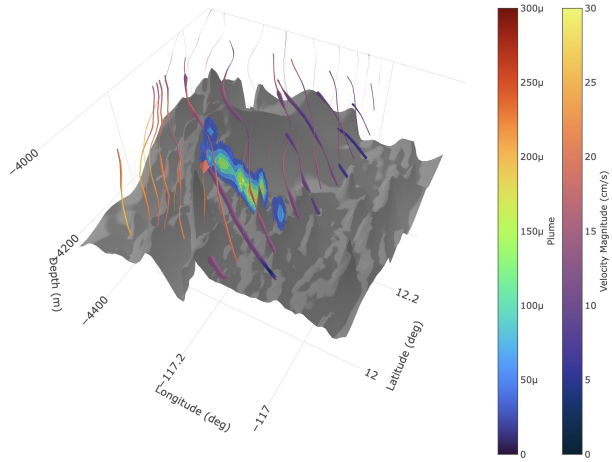

(b) View 2, with velocity streamtubes

Fig. 6: DSM Plume Forecast Experiment 2021. Two views of the interactive 3DSeaVizKit sediment plume visualization at 16Z on May 8th, 2021, as forecast by our MSEAS-PE ocean modeling system.

subject to variability.

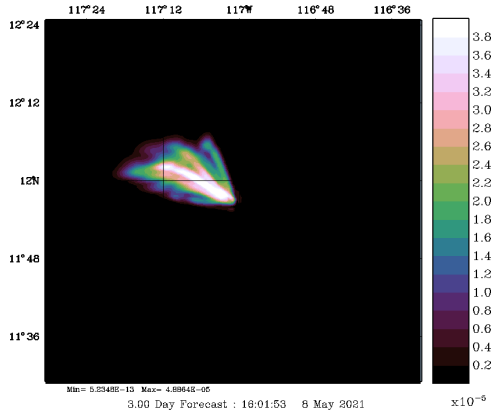

Fig. 7: DSM Plume Forecast Experiment 2021. NCAR visualizations of plume concentration uncertainty at 16Z on May 8th, 2021, as quantified by our real-time ESSE ensemble forecast.

C. DRI-CALYPSO Forecast Experiment 2022

The most recent application of our visualization suite was during a two-part real-time sea experiment in the Balearic Sea, first from February 18 to March 12, 2022, and again from March 25 to June 29, 2022. We issued real-time deterministic and probabilistic forecasts of ocean fields, as well as Lagrangian flow maps, coherent sets, subduction forecasts, and drifter forecasts [45]. The geographic modeling domain is shown in figure 1c with the sub-domain of interest for subduction dynamics highlighted in red.

For this experiment, the MSEAS modeling system was set up in an implicit 2-way nesting configuration (900 m resolution Balearic Sea domain and a 300 m resolution process domain). The ocean forecasts were initialized from WMOP [61], downscaled to higher resolution and updated with ocean data from varied open sources of opportunity (CTDs, ARGO floats [62], gliders, SST [63], etc.). Ensemble forecasts were initialized using ESSE procedures [51, 52], extended to multi-region uncertainty initialization. These ocean simulations were forced by atmospheric flux fields forecast by the Global Forecast System (GFS) $0.25°$ model from NCEP [60] and by tidal forcing from TPXO8 [55, 56], but adapted to the high-resolution bathymetry and coastlines [3, 34].

1) Ocean Physics: Each day during the first part of this experiment, we distributed visualizations of a central forecast of the ocean fields at 6-hour intervals for 6 days, using both NCAR Graphics and 2DSeaVizKit. The 900 m resolution density anomaly at the surface at 0Z on March 10, 2022 using 2DSeaVizKit is shown in figure 8a, while the density anomaly along a vertical section at $41.3°$N is shown in figure 8b. Notice the presence of several eddies along $41°$N, as well as strong density fronts in that region; these fronts indicate where subduction is expected to occur, and hence the dynamically active region where major experimental operations took place.

In the second part of the experiment, between April and June 2022, we issued forecasts of the depth of the $\sigma_\theta = 28.85$ isopycnal, and our forecasts were validated against data from a fleet of Spray gliders [64]. This particular isopycnal value was selected for studying frontal features and eddies in the region north of Mallorca. In figure 9, 3D velocity streamtubes and the $\sigma_\theta = 28.85$ isopycnal depth (orange surface) at 0Z on June 19, 2022 are illustrated, using 3DSeaVizKit. Notice the cyclonic eddy (around $40.5°$N, $3.25°$E) indicated by the velocity streamtubes. Cyclonic eddies generate upwelling in their centers and directly below this eddy we see a dome formation in the density anomaly. Adjacent to the eddy and dome is a very deep valley suggesting the presence subduction. Above the north wall of this valley is a ribbon of streamtubes, suggesting a density front associated with the subduction.

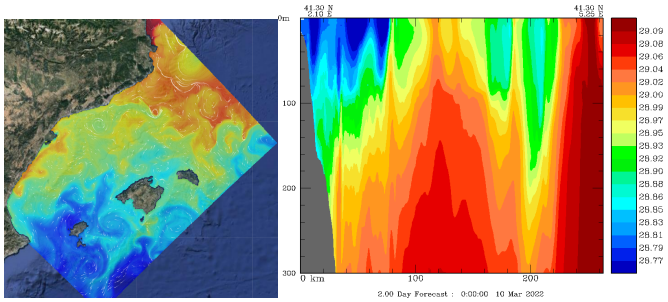

(a) Surface (2DSeaVizKit) (b) Vertical Section (NCAR Graphics)

Fig. 8: DRI-CALYPSO Forecast Experiment 2022. CALYPSO density anomaly at 0Z on March 10, 2022, as forecast by our MSEAS-PE ocean modeling system.

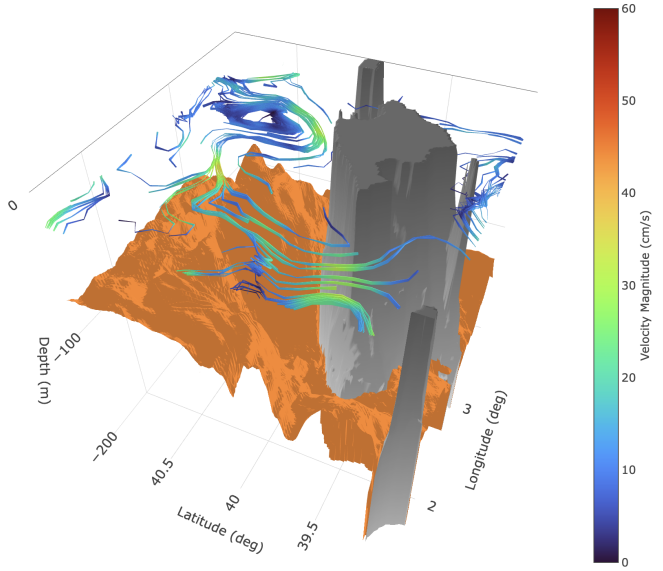

Fig. 9: DRI-CALYPSO Forecast Experiment 2022. Velocity streamtubes and $\sigma_\theta = 28.85$ isopycnal depth (orange surface) at 0Z on June 19, 2022, as forecast by our MSEAS-PE ocean modeling system.

2) Lagrangian Products: Each day, we used the forecasts generated by the MSEAS modeling system to obtain various derived products that help us better describe the flow.

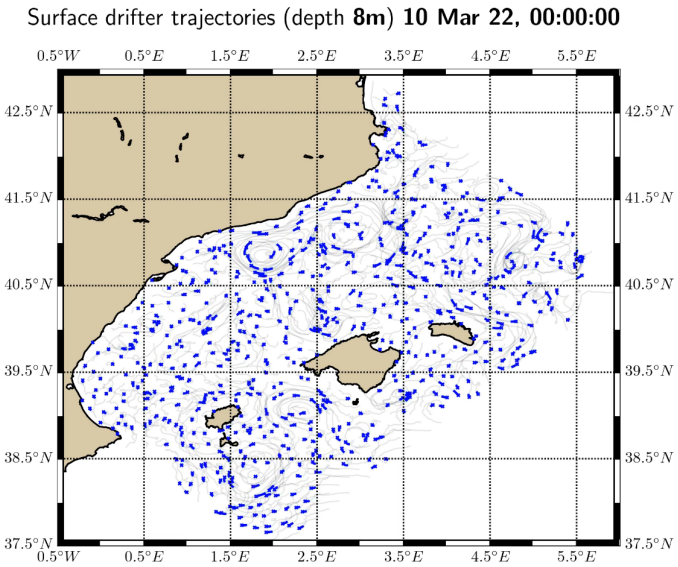

Fig. 10: DRI-CALYPSO Forecast Experiment 2022. Trajectories in the domain at the depth of 8m for the time interval above of 96 hours, with the tail corresponding to the trajectory in the last 24 hours, as forecast by our MSEAS-PE ocean modeling system.

The first of these is a plot (and movie [45]) of 2D drifter trajectories released in a uniform grid (figure 10). We initialized these drifters at various depths of interest corresponding to the drogue depths of various drifters released in the field [65]. This allows us evaluate the skill of our ocean flow field estimates and forecasts by comparing these trajectories to the trajectories of the real drifters.

The second set of products used to further study three-dimensional transport of water masses and subduction dynamics are based on flow maps that we compute. Specifically, the forward and backward flow maps across depth (z-flow map) best help identify the subduction regions. The 96-hour backward z-flow map on March 10, 2022 at 0Z and at 102 m (which shows the *initial* depth of each water parcel that ended up at 102 m after 4 days) is shown in figure 11. The dark red regions indicate water masses subducted from the surface to 102 m over 4 days; notice these are located near the fronts indicated in figure 8, as well as north of Mallorca, the other main location of at-sea operations.

The third set of quantities that we plot are indicators of Lagrangian Coherent Structures as they provide a skeleton of the flow. These include the FTLE and Dilation maps [44]. The 3D FTLE map (shown in figure 12a) specifies the amount of stretching of the flow map in the considered time interval. Specifically, the forward / backward 3D FTLE is a logarithmic scaling of the dominant singular values of the gradient forward / backward flow map with the time duration of interest. The forward FTLE ridges thus highlight codimension-one manifolds (curves in 2D, surfaces in 3D) that repel particles starting on either side, whereas the backward FTLE ridges highlight codimension-one manifolds that attract particles towards the

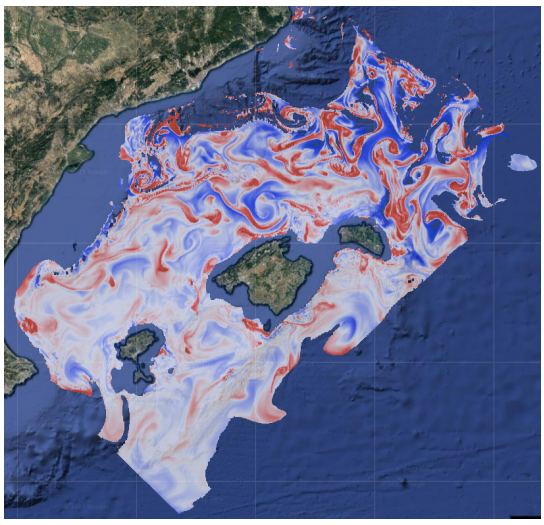

Fig. 11: DRI-CALYPSO Forecast Experiment 2022. CALYPSO 96-hour backward z-flow map at 0Z on March 10, 2022 at 102 m depth, as forecast by our MSEAS-PE ocean modeling system.

ridge that originally start far apart. Similarly, the dilation map (shown in figure 12b) is defined as the product of the singular values of the gradient of the flow map and quantifies the change in area of a water parcel.

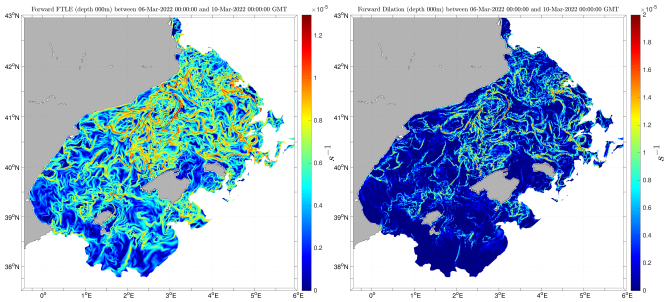

(a) Forward FTLE map (b) Dilation map

Fig. 12: DRI-CALYPSO Forecast Experiment 2022. Lagrangian Coherent structures for the CALYPSO domain, as forecast by our MSEAS-PE ocean modeling system.

Finally, we generate a set of plots (figure 13) that show the water volumes that are forecast to subduct in 3D from the surface layers to deeper layers. They illustrate in 3D+time where these waters start, how they move, and where they end up. The waters that are plotted in this subduction analysis are only the volumes of water that start within the upper ocean layers (above 15m depth) anywhere in our modeling domain and reach 50m after 4 days. This is all that is plotted, at 3 times (blue is day 0, green is day 2 and red is day 4).

IV. Conclusion

In this work, we have presented our MSEAS visualization suite, a collection of 2D and 3D multivariate visualization tools

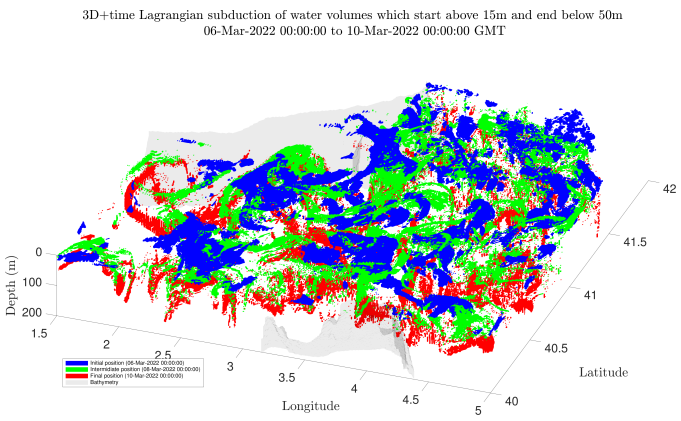

Fig. 13: DRI-CALYPSO Forecast Experiment 2022. Subduction analysis generated in MATLAB, using ocean fields forecast by our MSEAS-PE modeling system.

that produce static and interactive maps of ocean fields. The various tools are based on the NCAR Command Language (NCL) and MATLAB, in addition to the in-house 2DSeaVizKit and 3DSeaVizKit tools that we developed to offer an interactive user experience. The suite is built for the MSEAS-PE ocean model and provides several features including the standard 2D cross-sections for scalar-valued data; quiver plots, pathlines, and streamtubes for vector-valued data; Lagrangian products (such as trajectories, Lagrangian Coherent Structures, etc.) plotting functionalities; isosurfaces for 3D data; and an interactive graphical user interface for selecting the quantities, times, and sub-domains of interest.

Applications of our visualization suite were demonstrated for three sea experiments that took place in the Gulf of Mexico (GOM probabilistic hindcast experiment), the Clarion-Clipperton Fracture Zone in the Pacific Ocean (real-time DSM forecast experiment), and the Balearic Sea (real-time DRI-CALYPSO forecast experiment). We showcased the visualization features available in the suite and how they were used to investigate the regions of high uncertainty in the GOM hindcast and relate them to bathymetric effects and the dynamics of the Loop Current. Additionally, the deep-sea-mining plume dynamics were highlighted using the modular features of 3DSeaVizKit during the real-time DSM forecast experiment. The most recent applications of the visualization suite occurred during the real-time DRI-CALYPSO forecast experiment. Results helped address several goals of the experiment, including the investigation of the dynamics of flow subduction using standard 2D static plots as well as novel 3D isosurface visualization and Lagrangian analysis.

In each use case, we employed these tools in conjunction with one another to perform analyses and interpret data in a way that would not have been possible had we used any single tool in isolation. We submit that no single visualization technique is sufficient to encompass the demands of ocean forecasting. The versatility of the MSEAS visualization suite has been useful for our modeling research. We hope that it will become useful for the ocean modeling community in the future for the analysis of other datasets.

ACKNOWLEDGMENTS

We thank all members of the MSEAS group, past and present. We are grateful to the Office of Naval Research (ONR) for enabling our MSEAS modeling system and visualization suite development, and for partial research support under grants N00014-18-1-2781 (DRI-CALYPSO) and N00014-19-1-2693 (IN-BDA), and to the Understanding Gulf Ocean Systems (UGOS) program of the National Academies of Sciences, Engineering, and Medicine, for partial research support under grant 2018-2798-03, each to the Massachusetts Institute of Technology (MIT). We are also grateful to The 11th Hour Project of The Schmidt Family Foundation and the Benioff Foundation for partial research support. We also thank all of our DRI-CALYPSO, GOM, and DSM colleagues, including everyone that participated to the sea experiments. Finally, we thank the HYCOM team for their ocean fields, as well as NCEP and ECMWF for their atmospheric forcing forecasts.

REFERENCES

[1] E. Deleersnijder, V. Legat, and P. F. J. Lermusiaux, "Multi-scale modelling of coastal, shelf and global ocean dynamics," *Ocean Dynamics*, vol. 60, no. 6, pp. 1357–1359, Dec. 2010.

[2] P. J. Haley, Jr. and P. F. J. Lermusiaux, "Multiscale two-way embedding schemes for free-surface primitive equations in the "Multidisciplinary Simulation, Estimation and Assimilation System"," *Ocean Dynamics*, vol. 60, no. 6, pp. 1497–1537, Dec. 2010.

[3] P. J. Haley, Jr., A. Agarwal, and P. F. J. Lermusiaux, "Optimizing velocities and transports for complex coastal regions and archipelagos," *Ocean Modeling*, vol. 89, pp. 1–28, 2015.

[4] D. N. Subramani and P. F. J. Lermusiaux, "Risk-optimal path planning in stochastic dynamic environments," *Computer Methods in Applied Mechanics and Engineering*, vol. 353, pp. 391–415, Aug. 2019.

[5] M. Serra, P. Sathe, I. Rypina, A. Kirincich, S. D. Ross, P. Lermusiaux, A. Allen, T. Peacock, and G. Haller, "Search and rescue at sea aided by hidden flow structures," *Nature Communications*, vol. 11, pp. 1–7, 2020.

[6] T. Höllt, A. Magdy, P. Zhan, G. Chen, G. Gopalakrishnan, I. Hoteit, C. D. Hansen, and M. Hadwiger, "Ovis: A framework for visual analysis of ocean forecast ensembles," *IEEE Transactions on Visualization and Computer Graphics*, vol. 20, no. 8, pp. 1114–1126, 2014.

[7] S.-I. Saitoh, R. Mugo, I. N. Radiarta, S. Asaga, F. Takahashi, T. Hirawake, Y. Ishikawa, T. Awaji, T. In, and S. Shima, "Some operational uses of satellite remote sensing and marine gis for sustainable fisheries and aquaculture," *ICES Journal of Marine Science*, vol. 68, no. 4, pp. 687–695, 2011.

[8] D. R. Lipşa, R. S. Laramee, S. J. Cox, J. C. Roberts, R. Walker, M. A. Borkin, and H. Pfister, "Visualization for the physical sciences," in *Computer graphics forum*, vol. 31, no. 8. Wiley Online Library, 2012, pp. 2317–2347.

[9] J.-G. Lee and M. Kang, "Geospatial big data: challenges and opportunities," *Big Data Research*, vol. 2, no. 2, pp. 74–81, 2015.

[10] A. Pang *et al.*, "Visualizing uncertainty in geo-spatial data," in *Proceedings of the workshop on the intersections between geospatial information and information technology*, vol. 10, no. 1.20. National Research Council Arlington, VA, 2001, p. 3823.

[11] S. Djurcilov, K. Kim, P. F. J. Lermusiaux, and A. Pang, "Volume rendering data with uncertainty information," in *Data Visualization 2001*, ser. Joint Eurographics - IEEE TCVG Symposium

on Visualization, D. S. Ebert, J. M. Favre, and R. Peikert, Eds. Springer Vienna, 2001, pp. 243–252, 355–356.
[12] S. Djurcilov, K. Kim, P. Lermusiaux, and A. Pang, "Visualizing scalar volumetric data with uncertainty," *Computers and Graphics*, vol. 26, no. 2, pp. 239–248, 2002.
[13] W. H. Ali, M. H. Mirhi, A. Gupta, C. S. Kulkarni, C. Foucart, M. M. Doshi, D. N. Subramani, C. Mirabito, P. J. Haley, Jr., and P. F. J. Lermusiaux, "Seavizkit: Interactive maps for ocean visualization," in *OCEANS 2019 MTS/IEEE SEATTLE*. Seattle: IEEE, Oct. 2019, pp. 1–10.
[14] P. Lemenkova, "Processing oceanographic data by Python libraries NumPy, SciPy and Pandas," *Aquatic Research*, Apr. 2019.
[15] K. M. Thyng, C. A. Greene, R. D. Hetland, H. M. Zimmerle, and S. F. DiMarco, "True colors of oceanography: Guidelines for effective and accurate colormap selection," *Oceanography*, vol. 29, no. 3, pp. 9–13, September 2016. [Online]. Available: https://doi.org/10.5670/oceanog.2016.66
[16] M. Rautenhaus, M. Böttinger, S. Siemen, R. Hoffman, R. M. Kirby, M. Mirzargar, N. Röber, and R. Westermann, "Visualization in meteorology—a survey of techniques and tools for data analysis tasks," *IEEE Transactions on Visualization and Computer Graphics*, vol. 24, no. 12, pp. 3268–3296, 2018.
[17] H. Childs, E. Brugger, B. Whitlock, J. Meredith, S. Ahern, D. Pugmire, K. Biagas, M. Miller, C. Harrison *et al.*, "VisIt: An end-user tool for visualizing and analyzing very large data," *High Performance Visualization—Enabling Extreme-Scale Scientific Insight*, p. 357–372, 2012.
[18] J. Ahrens, B. Geveci, and C. Law, "ParaView: An end-user tool for large-data visualization," in *Visualization Handbook*, C. D. Hansen and C. R. Johnson, Eds. Burlington: Butterworth-Heinemann, 2005, pp. 717–731. [Online]. Available: https://www.sciencedirect.com/science/article/pii/B9780123875822500381
[19] M. Rautenhaus, M. Kern, A. Schäfler, and R. Westermann, "Three-dimensional visualization of ensemble weather forecasts – part 1: The visualization tool Met.3D (version 1.0)," *Geoscientific Model Development*, vol. 8, no. 7, p. 2329–2353, 2015. [Online]. Available: https://www.geosci-model-dev.net/8/2329/2015/
[20] C. Helbig, L. Bilke, H.-S. Bauer, M. Böttinger, and O. Kolditz, "MEVA-an interactive visualization application for validation of multifaceted meteorological data with multiple 3d devices," *PloS one*, vol. 10, no. 4, p. e0123811, 2015.
[21] M. Koutek, F. Debie, and I. Van der Neut, "3D exploration of meteorological data: Facing the challenges of operational forecasters," in *EGU General Assembly Conference Abstracts*, 2016, pp. EPSC2016–8398.
[22] R. Schlitzer, "Interactive analysis and visualization of geoscience data with ocean data view," *Computers & Geosciences*, vol. 28, no. 10, pp. 1211 – 1218, 2002, shareware and freeware in the Geosciences II. A special issue in honour of John Butler. [Online]. Available: http://www.sciencedirect.com/science/article/pii/S0098300402000407
[23] S. Li, S. Jaroszynski, S. Pearse, L. Orf, and J. Clyne, "VAPOR: A visualization package tailored to analyze simulation data in earth system science," *Atmosphere*, vol. 10, no. 9, 2019. [Online]. Available: https://www.mdpi.com/2073-4433/10/9/488
[24] Computational & Information Systems Laboratory, NCAR, "The NCAR Command Language," 2019. [Online]. Available: http://dx.doi.org/10.5065/D6WD3XH5
[25] T. M. Inc., "MATLAB," 2022. [Online]. Available: https://www.mathworks.com/products/matlab.html
[26] Y. Gao, W. H. Ali, C. Foucart, C. Mirabito, P. J. Haley, Jr., and P. F. J. Lermusiaux, "3DSeaVizKit: An interactive spatiotemporal visualization toolkit for ocean data," 2022, in preparation.
[27] W. G. Leslie, A. R. Robinson, P. J. Haley, Jr, O. Logutov, P. A. Moreno, P. F. J. Lermusiaux, and E. Coelho, "Verification and training of real-time forecasting of multi-scale ocean dynamics for maritime rapid environmental assessment," *Journal of Marine Systems*, vol. 69, no. 1, pp. 3–16, 2008.
[28] P. J. Haley, Jr., P. F. J. Lermusiaux, A. R. Robinson, W. G. Leslie, O. Logoutov, G. Cossarini, X. S. Liang, P. Moreno, S. R. Ramp, J. D. Doyle, J. Bellingham, F. Chavez, and S. Johnston, "Forecasting and reanalysis in the Monterey Bay/California Current region for the Autonomous Ocean Sampling Network-II experiment," *Deep Sea Research Part II: Topical Studies in Oceanography*, vol. 56, no. 3–5, pp. 127–148, Feb. 2009.
[29] P. F. J. Lermusiaux, D. N. Subramani, J. Lin, C. S. Kulkarni, A. Gupta, A. Dutt, T. Lolla, P. J. Haley, Jr., W. H. Ali, C. Mirabito, and S. Jana, "A future for intelligent autonomous ocean observing systems," *Journal of Marine Research*, vol. 75, no. 6, pp. 765–813, Nov. 2017, the Sea. Volume 17, The Science of Ocean Prediction, Part 2.
[30] D. N. Subramani, P. J. Haley, Jr., and P. F. J. Lermusiaux, "Energy-optimal path planning in the coastal ocean," *Journal of Geophysical Research: Oceans*, vol. 122, pp. 3981–4003, 2017.
[31] C. S. Kulkarni, P. J. Haley, Jr., P. F. J. Lermusiaux, A. Dutt, A. Gupta, C. Mirabito, D. N. Subramani, S. Jana, W. H. Ali, T. Peacock, C. M. Royo, A. Rzeznik, and R. Supekar, "Real-time sediment plume modeling in the Southern California Bight," in *OCEANS Conference 2018*. Charleston, SC: IEEE, Oct. 2018.
[32] A. Gupta, P. J. Haley, D. N. Subramani, and P. F. J. Lermusiaux, "Fish modeling and Bayesian learning for the Lakshadweep Islands," in *OCEANS 2019 MTS/IEEE SEATTLE*. Seattle: IEEE, Oct. 2019, pp. 1–10.
[33] P. F. J. Lermusiaux, M. Doshi, C. S. Kulkarni, A. Gupta, P. J. Haley, Jr., C. Mirabito, F. Trotta, S. J. Levang, G. R. Flierl, J. Marshall, T. Peacock, and C. Noble, "Plastic pollution in the coastal oceans: Characterization and modeling," in *OCEANS 2019 MTS/IEEE SEATTLE*. Seattle: IEEE, Oct. 2019, pp. 1–10.
[34] O. G. Logutov and P. F. J. Lermusiaux, "Inverse barotropic tidal estimation for regional ocean applications," *Ocean Modelling*, vol. 25, no. 1–2, pp. 17–34, 2008. [Online]. Available: http://www.sciencedirect.com/science/article/pii/S1463500308000851
[35] A. Agarwal and P. F. J. Lermusiaux, "Statistical field estimation for complex coastal regions and archipelagos," *Ocean Modelling*, vol. 40, no. 2, pp. 164–189, 2011.
[36] P. F. J. Lermusiaux, "Evolving the subspace of the three-dimensional multiscale ocean variability: Massachusetts Bay," *Journal of Marine Systems*, vol. 29, no. 1, pp. 385–422, 2001.
[37] P. F. J. Lermusiaux, "Uncertainty estimation and prediction for interdisciplinary ocean dynamics," *Journal of Computational Physics*, vol. 217, no. 1, pp. 176–199, 2006.
[38] P. F. J. Lermusiaux, "Estimation and study of mesoscale variability in the Strait of Sicily," *Dynamics of Atmospheres and Oceans*, vol. 29, no. 2, pp. 255–303, 1999.
[39] P. F. J. Lermusiaux, "Adaptive modeling, adaptive data assimilation and adaptive sampling," *Physica D: Nonlinear Phenomena*, vol. 230, no. 1, pp. 172–196, 2007.
[40] Computational & Information Systems Laboratory, NCAR, "NCAR Graphics," 2022. [Online]. Available: http://ngwww.ucar.edu/index.html
[41] P. F. J. Lermusiaux and C.-S. Chiu, "Four-dimensional data assimilation for coupled physical-acoustical fields," in *Acoustic Variability, 2002*, N. G. Pace and F. B. Jensen, Eds. Saclantcen: Kluwer Academic Press, 2002, pp. 417–424.
[42] G. Haller, "Lagrangian coherent structures," *Annual Review of Fluid Mechanics*, vol. 47, no. 1, pp. 137–162, 2015.
[43] S. C. Shadden, "Lagrangian coherent structures," in *Transport*

and Mixing in Laminar Flows. John Wiley & Sons, Ltd, 2011, pp. 59–89.
[44] H. S. Huntley, B. L. Lipphardt Jr., G. Jacobs, and A. D. Kirwan Jr., "Clusters, deformation, and dilation: Diagnostics for material accumulation regions," *Journal of Geophysical Research: Oceans*, vol. 120, no. 10, pp. 6622–6636, 2015.
[45] MSEAS Group, "CALYPSO Real-Time Balearic Sea Experiment 2022," 2022. [Online]. Available: http://mseas.mit.edu/Sea_exercises/CALYPSO/2022/
[46] P. Crickard III, *Leaflet. js essentials*. Packt Publishing Ltd, 2014.
[47] N. Q. Zhu, *Data visualization with D3. js cookbook*. Packt Publishing Ltd, 2013.
[48] Plotly Technologies Inc. (2015) Collaborative data science. Montreal, QC. [Online]. Available: https://plot.ly
[49] GEBCO Compilation Group, "The GEBCO_2022 grid," 2022.
[50] E. P. Chassignet, H. E. Hurlburt, O. M. Smedstad, G. R. Halliwell, P. J. Hogan, A. J. Wallcraft, R. Baraille, and R. Bleck, "The HYCOM (Hybrid Coordinate Ocean Model) data assimilative system," *Journal of Marine Systems*, vol. 65, no. 1-4, pp. 60–83, 2007.
[51] P. F. J. Lermusiaux, D. G. M. Anderson, and C. J. Lozano, "On the mapping of multivariate geophysical fields: Error and variability subspace estimates," *Quarterly Journal of the Royal Meteorological Society*, vol. 126, no. 565, pp. 1387–1429, 2000.
[52] P. F. J. Lermusiaux, "On the mapping of multivariate geophysical fields: Sensitivities to size, scales, and dynamics," *Journal of Atmospheric and Oceanic Technology*, vol. 19, no. 10, pp. 1602–1637, 2002.
[53] National Centers for Environmental Prediction (NCEP), "Climate forecast system (CFS)," https://www.ncei.noaa.gov/products/weather-climate-models/climate-forecast-system, Sep. 2021.
[54] European Centre for Medium-Range Weather Forecasts (ECMWF), "ECMWF reanalysis v5 (era5)," https://www.ecmwf.int/en/forecasts/datasets/reanalysis-datasets/era5, Sep. 2021.
[55] G. D. Egbert and S. Y. Erofeeva, "Efficient inverse modeling of barotropic ocean tides," *J. Atmos. Ocean. Technol.*, vol. 19, no. 2, pp. 183–204, 2002.
[56] ——, "OSU tidal inversion," http://volkov.oce.orst.edu/tides/tpxo8_atlas.html, 2013.
[57] MSEAS Group, "Deep Sea Mining CCFZ Experiment 2021," 2021. [Online]. Available: http://mseas.mit.edu/Sea_exercises/DSM21
[58] D. J. Amon, A. Hilario, P. M. Arbizu, and C. R. Smith, "Observations of organic falls from the abyssal Clarion-Clipperton Zone in the tropical eastern Pacific Ocean," *Marine Biodiversity*, vol. 47, no. 2, pp. 311–321, 2017.
[59] C. Hauton, A. Brown, S. Thatje, N. C. Mestre, M. J. Bebianno, I. Martins, R. Bettencourt, M. Canals, A. Sanchez-Vidal, B. Shillito *et al.*, "Identifying toxic impacts of metals potentially released during deep-sea mining—a synthesis of the challenges to quantifying risk," *Frontiers in Marine Science*, vol. 4, p. 368, 2017.
[60] National Centers for Environmental Prediction (NCEP), "Global forecast system (GFS)," https://www.emc.ncep.noaa.gov/index.php?branch=GFS, Aug. 2018.
[61] M. Juza, B. Mourre, L. Renault, S. Gómara, K. Sebastián, S. Lora, J. P. Beltran, B. Frontera, B. Garau, C. Troupin *et al.*, "Socib operational ocean forecasting system and multiplatform validation in the western mediterranean sea," *Journal of Operational Oceanography*, vol. 9, no. sup1, pp. s155–s166, 2016.
[62] Argo, "Argo float data and metadata from global data assembly centre (argo gdac)," 2000, sEANOE.
[63] F. Monaldo, "Primer on the estimation of sea surface temperature using Terascan processing of NOAA AVHRR satellite data," http://fermi.jhuapl.edu/avhrr/primer/primer_html.html, Jan. 1996.
[64] D. L. Rudnick, "Spray," 2022. [Online]. Available: http://chowder.ucsd.edu/Rudnick/Spray.html
[65] Woods Hole Oceanographic Institute (WHOI), "CALYPSO 2019 fieldwork," 2019. [Online]. Available: https://calypsodri.whoi.edu/category/2019-fieldwork/